FFLO state driven by quasiperiodic Zeeman field and its transition to localized states

Xingbo Wei [1,2] and W. Zhu [2,*]

[1] *Department of Physics, Zhejiang University, Hangzhou 310027, China*

[2] *Key Laboratory for Quantum Materials of Zhejiang Province, School of Science, Westlake University, Hangzhou 310024, China*

(Received 12 October 2021; revised 7 January 2022; accepted 2 March 2022; published 14 March 2022)

We numerically study the ground-state properties of a one-dimensional lattice model in the presence of a quasiperiodic Zeeman field, by means of the density matrix renormalization group algorithm. We map out a global phase diagram, which encloses a Bardeen-Cooper-Schrieffer (BCS) phase, a Fulde-Ferrell-Larkin-Ovchinnikov (FFLO) phase where the Cooper pairs obtain a finite center-of-mass momentum, and a localized phase. The FFLO phase is promoted by the quasiperiodic Zeeman field, which demonstrates a power-law pairing correlation with a critical exponent $\eta_{\mathrm{FFLO}} < 1$ decaying much slower than the charge density and spin density correlations. By tuning the interaction and the filling factor, we find the FFLO phase is suppressed in the strong interaction and low filling regions. A large Zeeman field destroys the FFLO state and drives a superconductor-insulator transition. Furthermore, we propose this FFLO phase and the superconductor-insulator transition could be observed in the optical lattice experiment.

DOI: 10.1103/PhysRevB.105.094203

I. INTRODUCTION

For conventional Bardeen-Cooper-Schrieffer (BCS) superconductors [1], the external magnetic field tends to destroy superconductivity owing to the Pauli paramagnetic depairing effect. Therefore, in general magnetism suppresses superconductivity in BCS superconductors. Interestingly, different from BCS homogeneous superconductors, the spin-imbalanced fermions induced by the uniform magnetic field allow exotic superconducting pairing states such as the Sarma state [2] and the Fulde-Ferrell-Larkin-Ovchinnikov (FFLO) state [3,4]. The FFLO state encloses the Cooper pairs with a finite center-of-mass momentum and spatially dependent order parameters $\Delta(\mathbf{r}) = \Delta e^{i\mathbf{q}\cdot\mathbf{r}}$ for FF states and $\Delta(\mathbf{r}) = \Delta(e^{i\mathbf{q}\cdot\mathbf{r}} + e^{-i\mathbf{q}\cdot\mathbf{r}})/2 = \Delta\cos(\mathbf{q}\cdot\mathbf{r})$ for LO states [5–7]. Especially, the recently identified "pair-density-wave" superconductors correspond to a special class of LO states [8]. In the past several decades, many efforts have been made to search for the FFLO phase, and many signatures have been observed in the layered organic superconductors [9–12] and heavy-fermion superconductors [13,14]. However, limited by the complexity of strongly correlated materials, so far unambiguous and direct experimental evidence for the FFLO phase remains limited. Thus, to design new experimental platforms is a possible way out for the detection of the FFLO phase.

In addition to the external magnetic field, another factor that could suppress BCS superconductors is randomness or disorder. Superconductors with disordered impurities are also known as dirty superconductors [15,16]. Intuitively, disorder increases resistance, whereas superconductivity has zero resistance, thus there is a competition between them. The original description of dirty superconductors is based on the Anderson theorem [15], which shows that superconductivity is insensitive to nonmagnetic impurities. However, later it has been realized that this theorem is flawed due to the unjustified assumption of homogeneous BCS pairing function near the metal-insulator transition [17]. Therefore, a superconductor-insulator transition is expected in dirty superconductors [18–20]. Interestingly, under certain conditions, one also finds disorder could enhance superconductivity [21–23]. Moreover, disorder may produce many interesting phenomena, e.g., disorder raises the critical temperature of the superconductor [23–26] and disorder results in the formation of superconducting islands [27].

In comparison to the uniform magnetic field and disorder, the random Zeeman field is more interesting since it has both magnetic and disordered properties. To our best knowledge, the influence of the uniform Zeeman field and the single magnetic impurity on exotic superconducting states have been studied before [28,29], but that of the random Zeeman field has not been addressed. In this paper, we study the effect of a quasiperiodic Zeeman field, a special type of random field accessible in the optical lattice, on superconductivity. The quasiperiodic Zeeman field has the feature of the random Zeeman field. When it is strong enough, the quasiperiodic Zeeman field is expected to induce localization [30–32]. Meanwhile, since the quasiperiodic Zeeman field has an approximate period, it can also induce the characteristics of the commensurate field. Due to this reason, the quasiperiodic Zeeman field should escape from Imry-Ma argument [33], which predicts that the superconducting order is fragile in the one-dimensional system with a random independent Zeeman field [34]. To clarify the relationship between the quasiperiodic Zeeman field and superconductivity is the motivation of this work.

The main result is that we map out a global phase diagram as shown in Fig. 1. We confirm that a quasiperiodic

*zhuwei@westlake.edu.cn

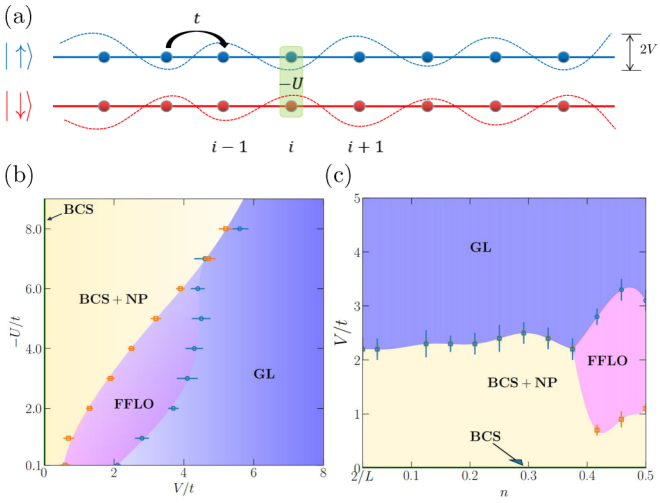

FIG. 1. (a) The schematic plot of a spin-dependent ladder with a quasiperiodic Zeeman field. The opposite spin parts interact via an attractive on-site interaction U. V is the amplitude of the quasiperiodic Zeeman field. (b) A $U-V$ phase diagram by setting the filling factor $n = 5/12$. (c) A $V-n$ phase diagram for $U = -1$. The error bars are from variances of 10 samples.

Zeeman field tends to destroy the BCS-type superconductor, and results in localization. Crucially, in the condition of small interaction regimes and near the half-filling case, there is an intermediate phase in between the BCS-type superconductor and the localized phase. This intermediate phase exhibits quasi-long-ranged pairing correlation, with a finite center-of-mass momentum. Thus we determine this intermediate phase as a FFLO state. We also study the phase transition between different phases.

The paper is organized as follows. In Sec. II, we introduce the one-dimensional Fermi model with a quasiperiodic Zeeman field. In Sec. III, we present our core phase diagrams and analyze the differences between different phases. In Sec. IV, we study the correlation exponent and the local spin polarization of FFLO states. In Sec. V, we study the phase transitions by tuning the Zeeman field amplitude for weak and strong interactions. To contact with experiments, we study the effect of the harmonic trap in Sec. VI. Finally, we present the conclusion and discuss several interesting topics for future study in Sec. VII.

II. MODEL AND METHOD

We consider a lattice chain with L sites filled with N fermions. The Hamiltonian is given by

$$\hat{H} = -t \sum_{i,\sigma=\uparrow,\downarrow} (\hat{c}^{\dagger}_{i,\sigma}\hat{c}_{i+1,\sigma} + \text{H.c.}) + U \sum_{i} \hat{n}_{i,\uparrow}\hat{n}_{i,\downarrow} + \sum_{i} V \cos(2\pi\alpha i + \phi)(\hat{n}_{i,\uparrow} - \hat{n}_{i,\downarrow}), \quad (1)$$

where $\hat{c}^{\dagger}_{i,\sigma}(\hat{c}_{i,\sigma})$ creates (eliminates) a spin-σ fermion at the site i. $\hat{n}_{i,\sigma} = \hat{c}^{\dagger}_{i,\sigma}\hat{c}_{i,\sigma}$ is the occupation number operator. The hopping strength $t \equiv 1.0$ is set to be the energy unit. $U < 0$ represents the on-site attractive interaction. V is the amplitude of the quasiperiodic Zeeman field and the parameter α controls the incommensurate period of the Zeeman field. Typically, we choose typical values $\alpha = (\sqrt{5}-1)/2$ and $\alpha = 1/e$ in this work. In Appendix B, we demonstrate that this quasiperiodic Zeeman field is special to the FFLO state as discussed below. $\phi \in [0, 2\pi)$ is an arbitrary phase factor, and in this study we use 10 different configurations of different ϕ to get averaged results. We denote the filling factor as $n = N/2L = (N_{\uparrow} + N_{\downarrow})/2L = (n_{\uparrow} + n_{\downarrow})/2$, where N_{σ} is the number of spin-σ fermions and n_{σ} is the total occupation number. Without loss of generality, we set the total spin polarization $P = (N_{\uparrow} - N_{\downarrow})/(N_{\uparrow} + N_{\downarrow}) = 0.0$ and use open boundary conditions (OBCs).

TABLE I. The differences among BCS, FFLO, and GL phases. Correlations follow the power-law decay $\mathbf{r}^{-\eta}$ or the exponential decay $e^{-\mathbf{r}/\xi}$, respectively, where η and ξ are decay indexes. η_{BCS} and η_{FFLO} represent the decay indexes of BCS and FFLO, respectively.

	BCS	BCS+NP	FFLO	GL
$m_{\mathbf{j}} = n_{\mathbf{j}\uparrow} - n_{\mathbf{j}\downarrow}$	$=0$	$\neq 0$	$\neq 0$	$\neq 0$
$G(\mathbf{j}, \mathbf{j}+\mathbf{r})$	$\mathbf{r}^{-\eta_{\text{BCS}}}$	$\mathbf{r}^{-\eta_{\text{BCS}}}$	$\mathbf{r}^{-\eta_{\text{FFLO}}}$	$e^{-\mathbf{r}/\xi}$
$\mathbf{q} = \mathbf{k}_{\uparrow} - \mathbf{k}_{\downarrow}$	$=0$	$=0$	$\neq 0$	/

The Hamiltonian in Eq. (1) without the interaction ($U/t = 0.0$) for $\alpha = (\sqrt{5}-1)/2$ is known as the Aubry-André (AA) model and there is a transition from extended states for $V/t < 2.0$ to Anderson localized states for $V/t > 2.0$ [30]. Compared with the spin-↑ and spin-↓ fermions being subjected to the same potential, resulting in the fact that the interaction enhances the localization effect [35], the Zeeman field provides opposite potentials to different spin fermions, and one may expect that the interaction destroys localization. Furthermore, the effect of the periodic Zeeman field has been studied in Ref. [36], which reveals π phases in Fermionic superfluids. In our study, we focus on the impact of the quasiperiodic Zeeman field on superconductivity.

We study the ground state of Eq. (1) by the DMRG method [37–39]. The DMRG as a common method has been used to study superconductivity of one-dimensional systems in lots of work [40–49]. In our numerical calculations, we find that when the size is large enough, the transition point is not sensitive to the size, thus we choose a suitable size $L = 120$. Furthermore, we keep 800 states and use 80 sweeps resulting in the fact that the truncation error is about 10^{-9}. To avoid being trapping in local minima, we use the two-site optimization. The DMRG calculations are performed using the ALPS libraries. More tests on the possible finite-size effect are given in Appendixes D and E.

III. QUANTUM PHASE DIAGRAM

In Fig. 1(b), we show the phase diagram at a fixed charge density $n = 5/12$, which encloses three different phases: a BCS-type superconducting phase, a FFLO phase, and a ground-state localized (GL) phase. The GL phase refers to the localization in the ground state, whose typical characteristic is that the correlation function decays exponentially as shown in Table I. As V/t increases, the system undergoes a transition

from superconducting states to the GL phase. In the limit of the noninteracting case, the localization transition occurs at $V/t = 2.0$ [30]. Figure 1(b) shows that the interaction U/t gradually expands the nonlocalized regime, and drives nonlocalized states to form superconductivity. Interestingly, in the weak interaction case, there exist two different superconducting states: the BCS phase and the FFLO phase, i.e., the FFLO phase is sandwiched between BCS and GL. When the interaction is strong, a direct transition from the BCS to GL occurs without the FFLO in-between.

In Fig. 1(c), we study the effect of the filling factor on superconducting states for $U/t = -1.0$. The phase diagram is symmetric about $n = 1/2$ because of the particle-hole symmetry, thus we only show the phase diagram for $n < 1/2$. The minimum filling factor we calculate is $n = 2/L$, at which the critical point of the GL transition is at $V/t \approx 2.2$. Around the half-filling ($n = 1/2$), the FFLO phase is favored. As the filling factor decreases, the GL and BCS phases gradually encroach on the parameter space and FFLO states are suppressed. A direct transition from the BCS phase to GL appears in low filling regions.

Next we turn to clarify how we determine the different phases in the phase diagrams as described above. First of all, the superconducting phases are characterized by the quasi-long-ranged pair-pair correlation function, $G(\mathbf{j}, \mathbf{j}+\mathbf{r}) = \langle \hat{c}^\dagger_{\mathbf{j}\uparrow} \hat{c}^\dagger_{\mathbf{j}\downarrow} \hat{c}_{\mathbf{j}+\mathbf{r}\downarrow} \hat{c}_{\mathbf{j}+\mathbf{r}\uparrow} \rangle$ in the spatial space. That is, a superconducting phase in one dimension should exhibit a quasi-long-ranged correlation $G(\mathbf{j}, \mathbf{j}+\mathbf{r}) \sim 1/\mathbf{r}^\eta$ [50]. Especially, the Fourier spectrum $G(\mathbf{q}) = \frac{1}{2L} \sum_{\mathbf{j},\mathbf{r}} G(\mathbf{j}, \mathbf{j}+\mathbf{r}) e^{i\mathbf{q}\mathbf{r}}$ can distinguish the center-of-mass momentum of Cooper pairs [40,41]. The condensation with a nonzero finite momentum, usually with the sign change in the spatial oscillation of $G(\mathbf{j}, \mathbf{j}+\mathbf{r})$, is an important indicator for the FFLO state [40–49].

In Table I, we show the differences between various phases and corresponding details are shown in Fig. 2. For the BCS states for $V/t = 0$, the local spin polarization $m_\mathbf{j} = n_{\mathbf{j}\uparrow} - n_{\mathbf{j}\downarrow} = 0$ [blue triangle in Fig. 2(a)] and the pair-pair correlation function has a power-law decay $G(\mathbf{j}, \mathbf{j}+\mathbf{r}) \propto 1/\mathbf{r}^{\eta_{\rm BCS}}$ [blue triangle in Fig. 2(c)], where $\eta_{\rm BCS} < 1$ is an interaction-dependent Luttinger-liquid dimensionless parameter [50–52]. After applying the Fourier transform, $G(\mathbf{q})$ only has a peak at $\mathbf{q}/\pi = 0$ in Fig. 2(d), indicating that the center-of-mass momentum is zero. As V/t increases, the quasiperiodic Zeeman field induces the local spin polarization $m_\mathbf{j} \neq 0$ and partial Cooper pairs are broken. Although the balanced population is destroyed at all sites for $V/t = 0.3$ in Fig. 2(a), $|G(\mathbf{j}, \mathbf{j}+\mathbf{r})|$ still decays algebraically as shown in Fig. 2(c), which manifests that it is still a superconducting state. Figure 2(d) shows that $G(\mathbf{q})$ only has a peak at $\mathbf{q}/\pi = 0$ for $V/t = 0.3$, indicating that the superconducting state is still a BCS state. We define such a phase as the coexistence of BCS and normal polarization (NP), in which Cooper pairs and unpaired fermions coexist [53]. Its typical characteristics are shown in Table I.

Similar to the BCS phase, the FFLO phase also exhibits the correlation with a power-law decay $G(\mathbf{j}, \mathbf{j}+\mathbf{r}) \propto \cos(\mathbf{q}\mathbf{r})/\mathbf{r}^{\eta_{\rm FFLO}}$ [52], where $\eta_{\rm FFLO}$ is an exponent related to the total spin polarization P. Typically, the correlation of the FFLO state for $V/t = 2.0$ is shown in Fig. 2(b), in which $G(\mathbf{j}, \mathbf{j}+\mathbf{r})$ fluctuates around zero. The corresponding $G(\mathbf{q})$

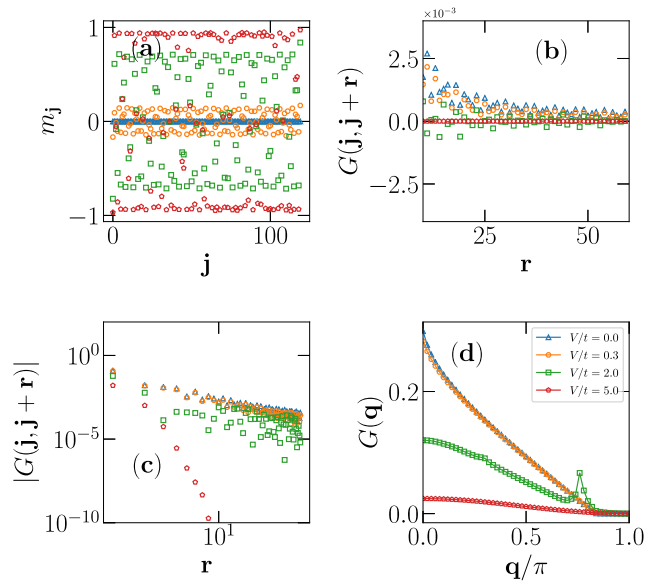

FIG. 2. (a) The local spin polarization $m_\mathbf{j} = n_{\mathbf{j}\uparrow} - n_{\mathbf{j}\downarrow}$ for different $V/t = 0.0$ (blue triangular), 0.3 (brown circles), 2.0 (green squares), and 5.0 (red pentagons). (b) and (c) The spatial space distributions of the pair-pair function $G(\mathbf{j}, \mathbf{j}+\mathbf{r})$ with $\mathbf{j} = 60$ in the linear scale and in the logarithmic scale, respectively. (d) The Fourier spectrum of the pair-pair function. Here we set $L = 120$, $n = 5/12$, $U/t = -1.0$, $\alpha = (\sqrt{5}-1)/2$, and $\phi = 0.0$.

has two peaks at $\mathbf{q}/\pi \approx 0.29$ and $\mathbf{q}/\pi \approx 0.76$ in Fig. 2(d), suggesting that Fermi surfaces are deformed and there are multiple effective center-of-mass momenta. Since the center-of-mass momentum $\mathbf{q} = |\mathbf{k}_\uparrow - \mathbf{k}_\downarrow| = |n_\uparrow - n_\downarrow|\pi$ [42,54–56] depends on the Fermi momentum of each species $\mathbf{k}_\uparrow$ and $\mathbf{k}_\downarrow$, one also expects that $m_\mathbf{j}$ fluctuates around $m_\mathbf{j} \approx \pm 0.29$ and $m_\mathbf{j} \approx \pm 0.76$, as shown in Fig. 2(a). In Fig. 1(b), FFLO states disappear in low filling regions since the reduction of the particle number leads to a decrease in the amplitude of $m_\mathbf{j}$, which reflects that the deformation of the Fermi surface decreases.

When the amplitude of the quasiperiodic Zeeman field is large enough, the quasi-long-ranged superconducting order is totally suppressed and the GL arises. In the localization region, $|G(\mathbf{j}, \mathbf{j}+\mathbf{r})|$ for $V/t = 5.0$ has an exponential decay as shown in Fig. 2(c). Meanwhile, the correlations of two fermionic species $G_\sigma(\mathbf{j}, \mathbf{j}+\mathbf{r}) = \langle \hat{c}^\dagger_{\mathbf{j}\sigma} \hat{c}_{\mathbf{j}+\mathbf{r}\sigma} \rangle$ also decay exponentially. Both $G(\mathbf{j}, \mathbf{j}+\mathbf{r})$ and $G_\sigma(\mathbf{j}, \mathbf{j}+\mathbf{r})$ indicate the same critical point in Fig. 4, which illustrates that there is no intermediate metallic "pseudogap" phase [35]. Fermions are localized by the quasiperiodic Zeeman field immediately after Cooper pairs are destroyed. This is due to the fact that the localization transition point $V/t \approx 2.8$ is larger than that of the AA model. $V/t \approx 2.8$ is strong enough to localize un-paired fermions; therefore there is no intermediate metallic phase.

IV. THE FFLO PHASE

In this section, we discuss some features of the FFLO phase in detail. First, we investigate the critical exponents of various correlation functions in the FFLO phase. The

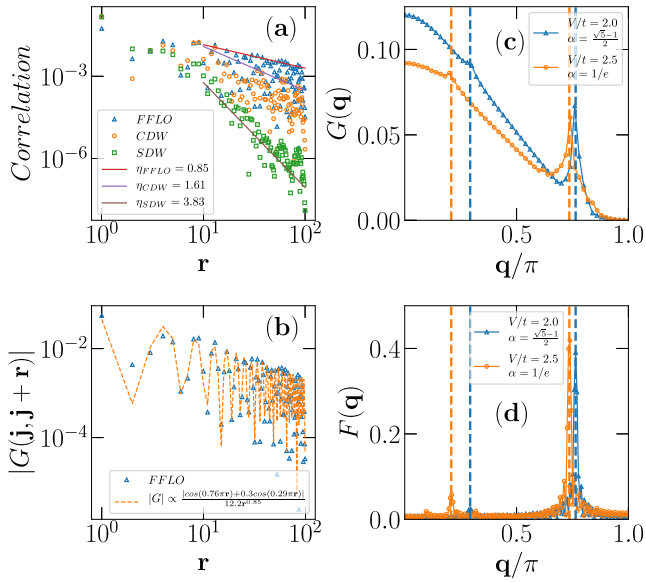

FIG. 3. (a) Comparison of the critical exponents of correlation functions. (b) The fitting of the pair-pair correlation in (a). (c) $G(\mathbf{q})$ for different irrational numbers α. (d) $F(\mathbf{q})$ for different irrational numbers α. The peaks in $G(\mathbf{q})$ have one-to-one correspondence with the most obvious peaks in $F(\mathbf{q})$: $\mathbf{q}/\pi = -2\alpha + 2 \approx 0.7639(3)$ for $\alpha = (\sqrt{5}-1)/2$ and $\mathbf{q}/\pi = 2\alpha \approx 0.7357(6)$ for $\alpha = 1/e$. Here we set $L = 120$, $n = 5/12$, $\phi = 0.0$, and $U/t = -1.0$. In (a) and (b), $V/t = 2.0$, $\alpha = (\sqrt{5}-1)/2$, and $\mathbf{j} = 19$.

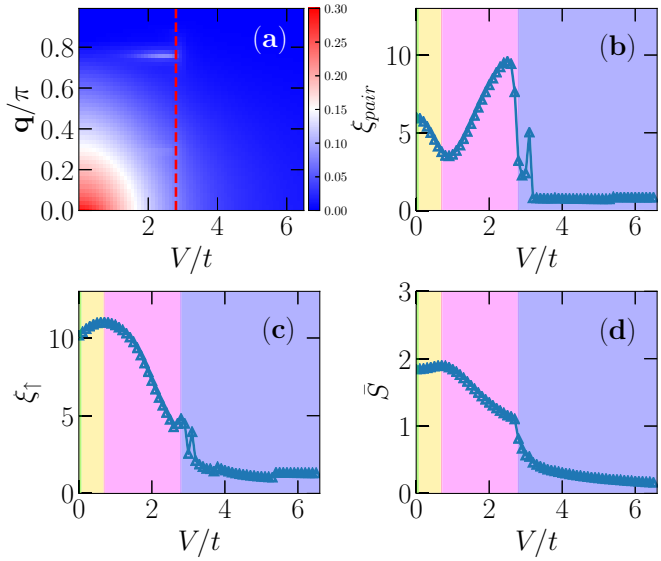

FIG. 4. The behaviors of different quantities as a function of V/t for the weak interaction $U/t = -1.0$. (a) Scan of $G(\mathbf{q})$ as a function of V/t. (b) ξ_{pair} as a function of V/t. (c) $\xi_\uparrow$ as a function of V/t. (d) Entanglement entropy S as a function of V/t. Here we set $L = 120$, $n = 5/12$, $\alpha = (\sqrt{5}-1)/2$, and $\phi = 0.0$. The color represents the value of $G(\mathbf{q})$ and the red dotted line marks $V/t \approx 2.8$ in (a). The color in (b)–(d) indicates different phases and the BCS phase is marked by the green shade.

correlation functions we study are the pair-pair correlation, the charge-density-wave (CDW) correlation $\langle \hat{n}_{\mathbf{j}}\hat{n}_{\mathbf{j}+\mathbf{r}}\rangle - \langle \hat{n}_{\mathbf{j}}\rangle\langle \hat{n}_{\mathbf{j}+\mathbf{r}}\rangle$, and the spin-density-wave (SDW) correlation $\langle \hat{m}_{\mathbf{j}}\hat{m}_{\mathbf{j}+\mathbf{r}}\rangle - \langle \hat{m}_{\mathbf{j}}\rangle\langle \hat{m}_{\mathbf{j}+\mathbf{r}}\rangle$. In Fig. 3(a), we find that all three correlation functions are site dependent, and have power-law decay. Crucially, their correlation exponents satisfy $\eta_{\text{SDW}} > \eta_{\text{CDW}} > \eta_{\text{FFLO}}$, indicating that superconductivity dominates over the other two orders. And in Fig. 3(b), we fit the pair-pair correlation and obtain the $|G| \propto |\cos(0.76\pi * \mathbf{r}) + 0.3\cos(0.29\pi\mathbf{r})|/\mathbf{r}^{0.85}$, giving the superconducting correlation exponent $\eta_{\text{FFLO}} \approx 0.85$. The observations of $\eta_{\text{FFLO}} < 1$, $\eta_{\text{CDW}} > 1$, and $\eta_{\text{SDW}} > 1$ indicate that the superconducting correlation dominates over the others [50–52]. We also notice that the product of η_{CDW} and η_{FFLO} exceeds unity in Fig. 3(a), deviation from the normal Luttinger liquid description [44,57–60]. As a comparison, it is worth stressing that for the FFLO state induced by the uniform Zeeman field, the FFLO state shows $\eta_{\text{FFLO}} > 1.0$ [44], which is much weaker than the present work. Thus, we conclude that the quasiperiodic Zeeman field tends to enhance the FFLO behavior.

Second, the local spin polarization of the FFLO state induced by uniform Zeeman fields has a characteristic wave vector $2\pi(n_\uparrow - n_\downarrow) = 2\mathbf{q}$ [61,62]. In contrast, when fermions are subjected to the quasiperiodic Zeeman field, the local spin polarization is modulated. In the ground state, fermions tend to occupy positions with low field energies when the Zeeman field dominates, thus we obtain $m_{\mathbf{j}} \approx \cos(2\pi\alpha\mathbf{j})$. Applying the Fourier transform $F(\mathbf{q}) = |\frac{1}{L}\sum_{\mathbf{j}} m_{\mathbf{j}} e^{i\mathbf{q}\cdot\mathbf{j}}|$, one can easily obtain the frequency of the local spin polarization at $\mathbf{q}/\pi = \pm 2\alpha + 2n$, where n is an integer. In Fig. 3(d), $\mathbf{q}$ corresponding to the most obvious peaks are instructed well. Furthermore, we find that the center-of-mass momentum of the FFLO state is consistent with the frequency of the local spin polarization. This consistency means that the local spin polarization induced by the Zeeman field is highly related to the center-of-mass momentum of the FFLO state. We confirm the above features by studying different αs, as shown in Figs. 3(c) and 3(d).

V. PHASE TRANSITIONS

In this section, we study the phase transitions by tuning the Zeeman field amplitude. We first introduce multiple physical quantities. The first one is the center-of-mass momentum $\mathbf{q}$, which relates to the peak location of $G(\mathbf{q})$. The second one is the effective correlation length ξ_{eff} [31,63], which is defined as

$$\xi_{\text{eff}} = \sqrt{\frac{\sum \mathbf{r}^2 |g(\mathbf{j},\mathbf{j}+\mathbf{r})|}{2\sum |g(\mathbf{j},\mathbf{j}+\mathbf{r})|}}, \tag{2}$$

where $g(\mathbf{j},\mathbf{j}+\mathbf{r})$ denotes the correlation function. In our study, we focus on two typical effective correlation lengths: ξ_{pair} and ξ_σ. ξ_{pair} is the effective correlation length of the pair-pair correlation function $g(\mathbf{j},\mathbf{j}+\mathbf{r}) = G(\mathbf{j},\mathbf{j}+\mathbf{r})$ and ξ_σ represents the effective correlation length of two fermionic species $g(\mathbf{j},\mathbf{j}+\mathbf{r}) = G_\sigma(\mathbf{j},\mathbf{j}+\mathbf{r}) = \langle \hat{c}^\dagger_{\mathbf{j}\sigma}\hat{c}_{\mathbf{j}+\mathbf{r}\sigma}\rangle$. In the GL phase, the pair-pair correlation function $G(\mathbf{j},\mathbf{j}+\mathbf{r}) \propto e^{-\mathbf{r}/\xi}$, whereas for superconducting states $G(\mathbf{j},\mathbf{j}+\mathbf{r}) \propto \mathbf{r}^{-\eta}$. Therefore, one may find the transition point of GL by ξ_{pair} effectively. Furthermore, we find it also indicates the transition from BCS-NP to FFLO well as shown in Fig. 4. In

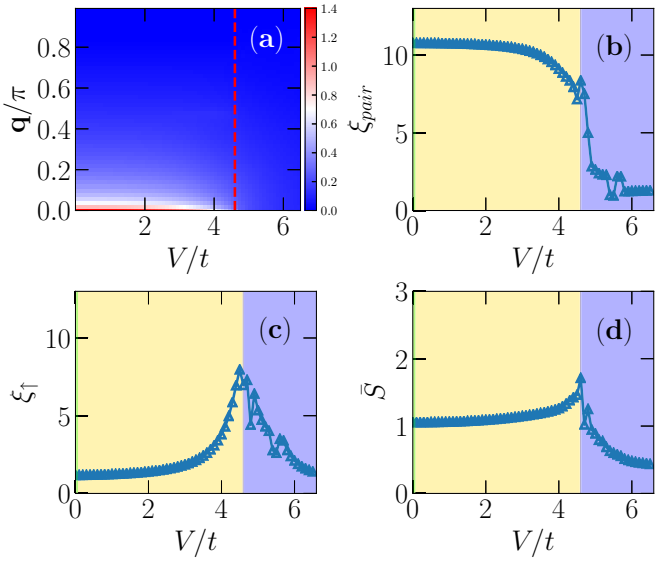

FIG. 5. The behaviors of different quantities as a function of V/t for the strong interaction $U/t = -7.0$. Here we set $L = 120$, $n = 5/12$, $\alpha = (\sqrt{5}-1)/2$, and $\phi = 0.0$. The quantities are the same as those in Fig. 4.

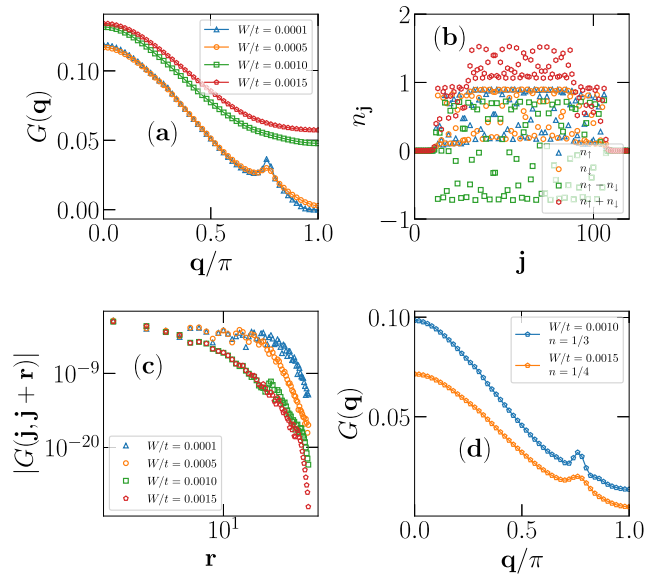

FIG. 6. (a) $G(\mathbf{q})$ for different W/ts. (b) Densities for $W/t = 0.0015$. (c) The decay behaviors of $|G(\mathbf{j},\mathbf{j}+\mathbf{r})|$ for different W/ts. (d) $G(\mathbf{q})$ for different W/ts and ns. $L = 120$, $U/t = -1.0$, $V/t = 2$, $\alpha = (\sqrt{5}-1)/2$, and $\phi = 0.0$. $n = 5/12$ in (a)–(c).

addition to the effective correlation length of the pair-pair correlation function ξ_{pair}, we also analyze ξ_σ. Since the behaviors of ξ_σ of different spin fermions are similar, we only show the result of spin-↑. To reduce the influence of the boundary, we only sum over two-thirds part of sites in the center of the chain. The last physical quantity is entanglement entropy $S = -\rho_A \log(\rho_A)$ [43], where $\rho_A = \text{Tr}_B[\rho_{AB}]$ is the reduced density matrix of the subsystem A. We calculate the mean entanglement entropy $\bar{S} = \langle S \rangle$, which averages all cut points from 1 to $L-1$.

In Fig. 4, we discuss the effect of the weak interaction. In Fig. 4(a), $G(\mathbf{q})$ has a peak at $\mathbf{q}/\pi = 0.0$ for BCS states, whereas that for FFLO states has a finite center-of-mass momentum. The most obvious peaks of $G(\mathbf{q})$ of FFLO states are at $\mathbf{q}/\pi = 2 - 2\alpha \approx 0.764$. After entering GL, peaks of $G(\mathbf{q})$ at $\mathbf{q}/\pi \neq 0$ are suppressed. In Figs. 4(b)–4(d), the trends of $\xi_\uparrow$ and $\bar{S}$ are similar, since they both characterize the property of nonpaired fermions. On the contrary, ξ_{pair} has an opposite behavior because it indicates the property of pairs. In the BCS-NP phase, ξ_{pair} reduces as V/t increases while $\xi_\uparrow$ and $\bar{S}$ grow, which indicates that pairs are destroyed by the quasiperiodic Zeeman field. When the amplitude V exceeds the critical value $V/t \approx 0.7$, ξ_{pair} increases, whereas $\xi_\uparrow$ and $\bar{S}$ reduces, the quasiperiodic Zeeman field instead promotes the formation of pairs, which suggests that the local spin polarization induced by the quasiperiodic Zeeman field promotes the formation of a new quasi-long-ranged order. For $V/t > 2.8$, the system enters GL, three physical quantities all have obvious reductions near the transition point.

In the strong interaction case, we find a transition from BCS-NP to GL appears and there is no FFLO in Fig. 5. In the process of the superconductor-insulator transition, there is no obvious peak formed at $\mathbf{q}/\pi \neq 0$ in Fig. 5(a). A simple understanding is that the interaction competes with the quasiperiodic Zeeman field and a large interaction would suppress the FFLO state and favor the normal BCS state. This is evidenced by the reduction of the amplitude of $m_\mathbf{j}$ in the strong interaction regime. The strong interaction makes the Cooper pairs more stable, therefore ξ_{pair} in Fig. 5(b) is much larger than that in Fig. 4(b). Meanwhile, $\xi_\uparrow$ is inhibited in Fig. 5(c), suggesting that $G_\sigma(\mathbf{j},\mathbf{j}+\mathbf{r}) = \langle \hat{c}^\dagger_{\mathbf{j}\sigma} \hat{c}_{\mathbf{j}+\mathbf{r}\sigma} \rangle$ has a fast decay. The strong interaction also results in the fact that the effective correlation length ξ_{pair} and ξ_σ have slower changes with V/t than those in the case of the weak interaction. In Fig. 5(d), $\bar{S}$ increases with V/t in the BCS-NP phase, whereas it reduces as V/t strengthens in the GL phase. This is consistent with the result of the weak interaction in Fig. 4(d).

VI. EXPERIMENTAL REALIZATION

The advantage of the current model is that it is accessible by ultracold Fermi gases with high controllability and tunability, which could be a new platform to search for the FFLO phase. Typically, the FFLO state can be realized by polarized ^{6}Li Fermi gas in one dimension and the phase diagram is consistent with the theoretical prediction [64]. The quasiperiodic Zeeman field can be regarded as spin-dependent potentials [65,66], which can be realized in optical lattices with ladder potentials as shown in Fig. 1(a). The quasiperiodic potentials can also be modulated, which are used to investigate the Anderson localization and many-body localization [67,68]. To make contact with experiments [64], we confine the Fermi gas in a harmonic trap,

$$H_{\text{trap}} = W \sum_{i=0}^{L-1} \left(i - \frac{L-1}{2} \right)^2 n_i, \tag{3}$$

where W is the strength of the trap. Figure 6(a) shows that peaks at $\mathbf{q}/\pi = 0.76$ gradually disappear as W/t increases. This is due to the harmonic trap increasing the effective

filling factor as shown in Fig. 6(b). As W/t increases, the short-distance decay behavior of $|G(\mathbf{j}, \mathbf{j}+\mathbf{r})|$ changes from a power-low decay to an exponential decay in Fig. 6(c), indicating that the deep trap promotes the occurrence of localization. The long-distance decay behaviors for different Ws all show exponential decays since the Fermi gas is bound in the center of the chain. To observe FFLO states experimentally, one may reduce the filling factor as W/t increases as shown in Fig. 6(d). This center-of-mass momentum of FFLO states can be directly probed by using the time-of-flight imaging in the experiments [20,69].

VII. DISCUSSION AND CONCLUSION

To summarize, we have studied the effect of the quasiperiodic Zeeman field on a one-dimensional lattice model. We demonstrate that a FFLO phase survives in the process of the superconductor-insulator transition. We find that both the strong interaction and low filling factor suppress the FFLO state. Unlike the FFLO states with a total spin polarization $P \neq 0$ induced by a uniform Zeeman field [40–49], the FFLO phase in the present work has $P = 0$. Furthermore, it is found that the correlation exponent of the FFLO state induced by the quasiperiodic Zeeman field exhibits $\eta_{\mathrm{FFLO}} < 1.0$, which is much stronger than that in the previous work [44]. Although the pairing occurs in momentum space, the center-of-mass momentum of FFLO can be modulated by the Zeeman field. A direct evidence is that the center-of-mass momentum of FFLO is the same as the frequency of the local spin polarization. In this study, we have used multiple physical quantities to characterize different phases. These physical quantities embody the competitive relationship among un-paired fermions, Cooper pairs, and the localization of both. Finally, we propose to realize the current lattice model using optical lattices in the experiment.

In this work, we have investigated the ground-state properties at zero temperature in the one-dimensional system. Regarding it as a starting point, many interesting topics can be derived, e.g., the competition between superconductivity and the quasiperiodic Zeeman field at finite temperature, the superconductivity in high-dimensional systems. In addition, superconducting properties of highly excited states and dynamic properties of superconductors are also interesting directions.

ACKNOWLEDGMENTS

The authors acknowledge insightful discussions with Xianlong Gao. This work was supported by "Pioneer" and "Leading Goose" R&D Program of Zhejiang (Grant No. 2022SDXHDX0005), the Key R&D Program of Zhejiang Province (Grant No. 2021C01002), and the foundation from Westlake University. We thank Westlake University HPC Center for computation support.

APPENDIX A: EFFECT OF THE PERIODIC ZEEMAN FIELD

In Fig. 7, we study the effect of the periodic Zeeman field on superconductivity. Figures 7(a) and 7(b) show $G(\mathbf{q})$ as a function of V/t for $U/t = -1.0$ and $U/t = -7.0$, respectively. In the case of the weak interaction for $U/t = -1.0$, the transition from BCS-NP to FFLO appears at $V/t \approx 1.3$, whereas it occurs at $V/t \approx 3.8$ for $U/t = -7.0$. A simple understanding is that the attractive interaction strengthens the Cooper pairs, so that a larger amplitude is needed to destroy Cooper pairs. The center-of-mass momentum of FFLO states is at $\mathbf{q}/\pi = 2\alpha = 1/2$, which is consistent with the wave vector of the periodic Zeeman field. Figures 7(c) and 7(d) show the mean entanglement entropy as a function of V/t for $U/t = -1.0$ and $U/t = -7.0$, respectively. In a weak periodic Zeeman field, BCS is destroyed to unpaired fermions and $\bar{S}$ grows as V/t increases. When the strength of the periodic Zeeman field exceeds the critical point, the Zeeman field promotes the generation of a new superconducting order. The Cooper pairs are re-formed and $\bar{S}$ decreases.

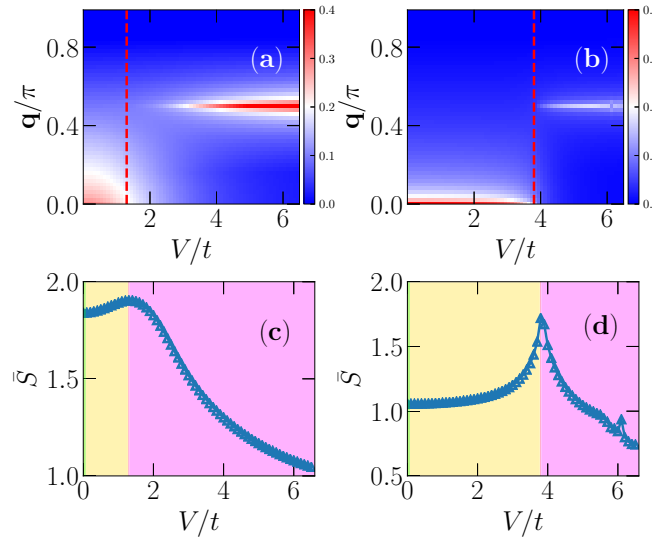

FIG. 7. $G(\mathbf{q})$ as a function of V/t for $U/t = -1.0$ and $U/t = -7.0$ in (a) and (b), respectively. The mean entanglement entropy as a function of V/t for $U/t = -1.0$ and $U/t = -7.0$ in (c) and (d), respectively. $L = 120$, $n = 5/12$, $\alpha = 1/4$, and $\phi = 0.0$. The green shade indicates the BCS phase in (c) and (d). The color represents the value of $G(\mathbf{q})$ in (a) and (b). The red dotted lines mark $V/t \approx 1.3$ and $V/t \approx 3.8$ in (a) and (b), respectively.

In Fig. 8, we show more details of FFLO states for $U/t = -1.0$. In Fig. 8(a), the fluctuation of $G(\mathbf{j}, \mathbf{j}+\mathbf{r})$ increases with V/t, manifesting that the periodic Zeeman field promotes the formation of FFLO states. Figure 8(b) shows that the correlation exponent reduces as V/t increases, which indicates that the strong periodic Zeeman field slows down the decay of the FFLO order. Moreover, the correlation exponent $\eta_{\mathrm{FFLO}} < 1$ is found for a large V/t. In Figs. 8(c) and 8(d), we study the Fourier transform of $G(\mathbf{j}, \mathbf{j}+\mathbf{r})$ and $m_{\mathbf{j}}$, respectively. They both display peaks at $\mathbf{q}/\pi = 2\alpha = 0.5$, which is consistent with the conclusion that FFLO states have the same frequency as those of the local spin polarization in the text.

APPENDIX B: EFFECT OF THE WHITE-NOISE-TYPE ZEEMAN FIELD

In the main text and previous section, we show that the most obvious center-of-mass momentum of the FFLO state

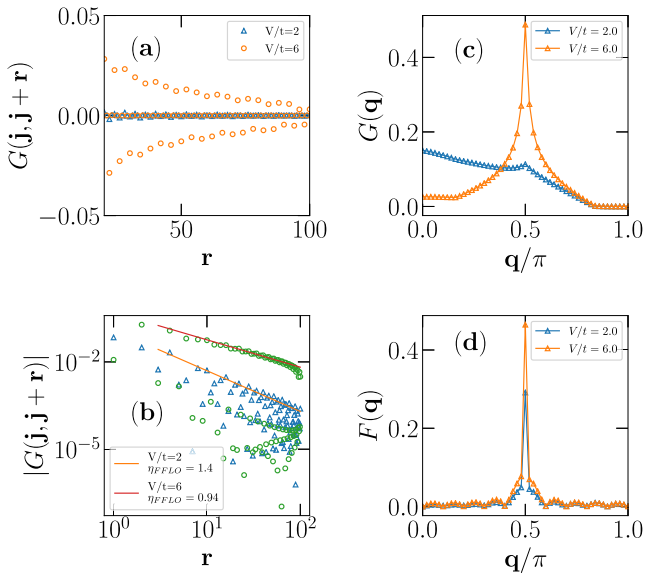

FIG. 8. (a) $G(\mathbf{j},\mathbf{j}+\mathbf{r})$ as a function of $\mathbf{r}$ with $\mathbf{j}=19$. (b) $|G(\mathbf{j},\mathbf{j}+\mathbf{r})|$ as a function of $\mathbf{r}$ with $\mathbf{j}=19$. (c) The Fourier transform of $G(\mathbf{j},\mathbf{j}+\mathbf{r})$. (d) The Fourier transform of the local spin polarization. $L=120$, $n=5/12$, $\alpha=1/4$, $U/t=-1$, and $\phi=0.0$.

is at $\mathbf{q}/\pi=\pm 2\alpha+2n$, which is related to the wave vector of the Zeeman field. A simple question that arises from this point is whether FFLO still exists when the Zeeman field is a white-noise-type Zeeman field. To address this question, we calculate the case of the random Zeeman field with a white noise distribution in Fig. 9. In Fig. 9(a), we show that $G(\mathbf{j},\mathbf{j}+\mathbf{r})$ fluctuates around zero, which indicates that the

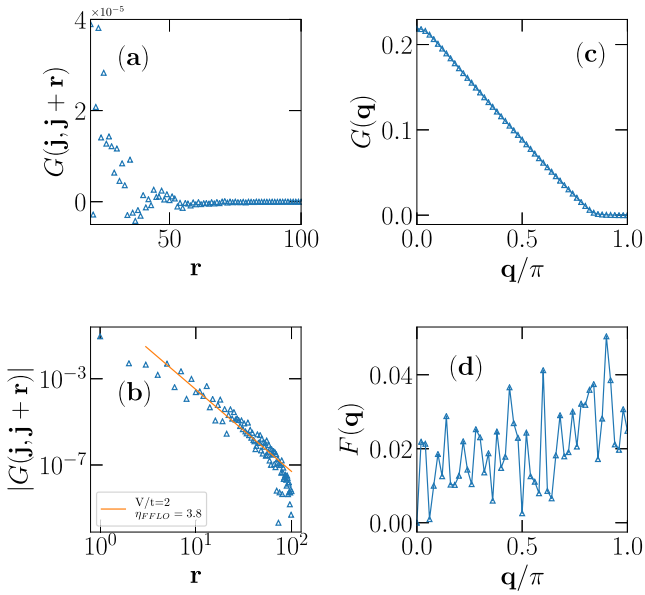

FIG. 9. (a) $G(\mathbf{j},\mathbf{j}+\mathbf{r})$ as a function of $\mathbf{r}$ with $\mathbf{j}=19$. (b) $|G(\mathbf{j},\mathbf{j}+\mathbf{r})|$ as a function of $\mathbf{r}$ with $\mathbf{j}=19$. (c) The Fourier transform of $G(\mathbf{j},\mathbf{j}+\mathbf{r})$. (d) The Fourier transform of the local spin polarization. $L=120$, $n=5/12$, $U/t=-1$, and the white-noise-type Zeeman field $V_i\in[-2,2]$.

order parameter has sign changes. In Fig. 9(b), we find that $|G(\mathbf{j},\mathbf{j}+\mathbf{r})|$ deviates from the power-low decay for large $\mathbf{r}$, which is consistent with the Imry-Ma-type argument [33]. The Fourier transform of $G(\mathbf{j},\mathbf{j}+\mathbf{r})$ has no obvious peak in Fig. 9(c). On the one hand, it is because the superconducting behavior is relatively weak, which can be evidenced by the decay behavior and superconducting correlation exponent, and on the other hand, it is because the order is random and there is no clear center-of-mass momentum. Figure 9(d) shows that $F(\mathbf{q})$ also has no obvious peak. This is due to the fact that the local spin polarization caused by the random Zeeman field is also random. In a word, here we show the white-noise-type Zeeman field leads to distinct physics, compared to the quasi-long-ranged Zeeman field as shown in the main text. This demonstrates that the quasiperiodic Zeeman field is important for FFLO states.

APPENDIX C: MEAN-FIELD RESULTS

In the main text, we use DMRG to study the effect of the quasiperiodic Zeeman field on superconductivity. Here we also use the mean-field approximation to study FFLO states. We do the mean-field approximation to the interaction term as

$$U\sum_i \hat{n}_{i\uparrow}\hat{n}_{i\downarrow} = \sum_i\left[\Delta^*\hat{c}_{i\downarrow}\hat{c}_{i\uparrow}+\hat{c}^\dagger_{i\uparrow}\hat{c}^\dagger_{i\downarrow}\Delta-\frac{\Delta^*\Delta}{U}\right], \quad \text{(C1)}$$

where $\Delta=U\langle\hat{c}_{i\downarrow}\hat{c}_{i\uparrow}\rangle$. When the order parameter Δ is real, the Hamiltonian reads

$$\begin{aligned}\widehat{H} = &-t\sum_{i,\sigma=\uparrow,\downarrow}\left(\hat{c}^\dagger_{i,\sigma}\hat{c}_{i+1,\sigma}+\text{H.c.}\right)\\ &+\sum_i V\cos(2\pi\alpha i+\phi)(\hat{n}_{i,\uparrow}-\hat{n}_{i,\downarrow})\\ &+\sum_i\left[\Delta\hat{c}_{i\downarrow}\hat{c}_{i\uparrow}+\Delta\hat{c}^\dagger_{i\uparrow}\hat{c}^\dagger_{i\downarrow}-\frac{\Delta^2}{U}\right]\\ &+\sum_i\mu(\hat{n}_{i,\uparrow}+\hat{n}_{i,\downarrow}),\end{aligned} \quad \text{(C2)}$$

where μ is the chemical potential to control the filling factor.

Next we will use a self-consistent method to solve Eq. (C2). We diagonalize the mean-field Hubbard Hamiltonian by a Bogoliubov transformation,

$$\begin{aligned}\hat{c}_\uparrow(i)&=\sum_n u_{n\uparrow}(i)\eta_n-v^*_{n\uparrow}(i)\eta^\dagger_n,\\ \hat{c}^\dagger_\uparrow(i)&=\sum_n u^*_{n\uparrow}(i)\eta^\dagger_n-v_{n\uparrow}(i)\eta_n,\\ \hat{c}_\downarrow(i)&=\sum_n u_{n\downarrow}(i)\eta_n+v^*_{n\downarrow}(i)\eta^\dagger_n,\\ \hat{c}^\dagger_\downarrow(i)&=\sum_n u^*_{n\downarrow}(i)\eta^\dagger_n+v_{n\downarrow}(i)\eta_n,\end{aligned} \quad \text{(C3)}$$

where $\eta^\dagger_n$ and η_n are quasiparticle operators. $u_{n\sigma}(i)$ and $v_{n\sigma}(i)$ satisfy

$$\sum_i u_{n\sigma}(i)^2+v_{n\sigma}(i)^2=1, \quad \text{(C4)}$$

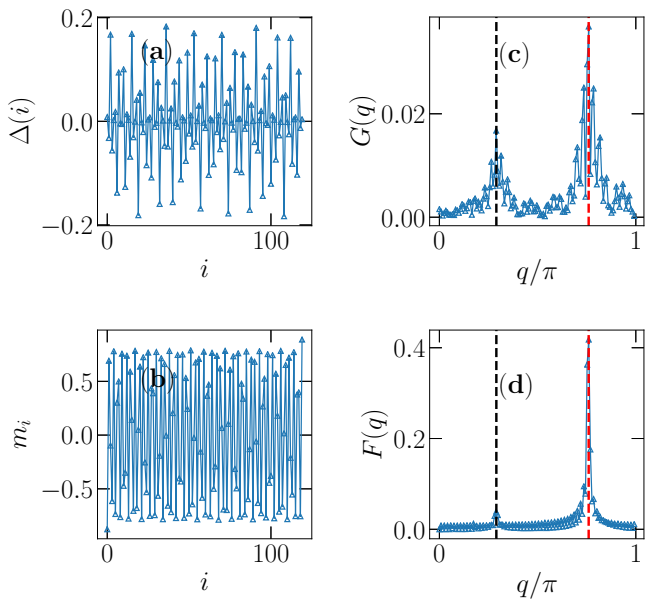

FIG. 10. $\Delta(i)$ and m_i as a function of i in (a) and (b), respectively. The Fourier transform of $\Delta(i)$ and m_i in (c) and (d), respectively. The black and red dotted lines mark $q/\pi = 0.29$ and $q/\pi = 0.76$, respectively. $L = 120$, $\mu = -0.183077595020778$ to make $n = 5/12$, $\alpha = (\sqrt{5}-1)/2$, $U/t = 1$, $V/t = 2$, and $\phi = 0.0$. Here we use OBCs.

which is from $\{\eta_n^\dagger, \eta_n\} = 1$. This yields the well-known Bogoliubov-de Gennes (BdG) equation,

$$\sum_j \begin{pmatrix} h_{ij\uparrow} & 0 & 0 & \delta_{ij} \\ 0 & h_{ij\downarrow} & \delta_{ij} & 0 \\ 0 & \delta_{ij}^* & -h_{ij\uparrow} & 0 \\ \delta_{ij}^* & 0 & 0 & -h_{ij\downarrow} \end{pmatrix} \begin{pmatrix} u_{n\uparrow}(j) \\ u_{n\downarrow}(j) \\ v_{n\uparrow}(j) \\ v_{n\downarrow}(j) \end{pmatrix} = E_n \begin{pmatrix} u_{n\uparrow}(i) \\ u_{n\downarrow}(i) \\ v_{n\uparrow}(i) \\ v_{n\downarrow}(i) \end{pmatrix}, \tag{C5}$$

where

$$h_\sigma u_{n\sigma}(i) = -t(u_{n\sigma}(i+1) + u_{n\sigma}(i-1)) + \sum_{i,\sigma}[V_\sigma cos(2\pi\alpha i + \phi) + \mu]u_{n\sigma}(i), \tag{C6}$$

and similarly for $v_{n\sigma}(i)$. In Eq. (C6), $V_\sigma = V$ for $\sigma = \uparrow$ and $V_\sigma = -V$ for $\sigma = \downarrow$. The self-consistency conditions of spin-$\uparrow$ densities expressed as

$$\begin{aligned} \langle n_{i\uparrow}\rangle &= \langle c_{i\uparrow}^\dagger c_{i\uparrow}\rangle \\ &= \frac{1}{2}\sum_n \langle [u_{n\uparrow}^*(i)\eta_n^\dagger - v_{n\uparrow}(i)\eta_n][u_{n\uparrow}(i)\eta_n - v_{n\uparrow}^*(i)\eta_n^\dagger]\rangle \\ &= \frac{1}{2}\sum_n [|u_{n\uparrow}(i)|^2\langle\eta_n^\dagger\eta_n\rangle + |v_{n\uparrow}(i)|^2\langle\eta_n\eta_n^\dagger\rangle] \\ &= \frac{1}{2}\sum_n [|u_{n\uparrow}(i)|^2 f(E_n) + |v_{n\uparrow}(i)|^2 f(-E_n)], \end{aligned} \tag{C7}$$

where $f(E) = 1/[1+\exp(E/k_BT)]$. The solutions of the BdG equations contain both positive and negative energies. Thus, we use the factor of $1/2$ to avoid double counting. Correspondingly, we can obtain the self-consistency conditions of spin-$\downarrow$ densities

$$\begin{aligned} \langle n_{i\downarrow}\rangle &= \langle c_{i\downarrow}^\dagger c_{i\downarrow}\rangle \\ &= \frac{1}{2}\sum_n [|u_{n\downarrow}(i)|^2 f(E_n) + |v_{n\downarrow}(i)|^2 f(-E_n)], \end{aligned} \tag{C8}$$

and those of the order parameter,

$$\begin{aligned} \Delta(i) &= U\langle\hat{c}_{i\downarrow}\hat{c}_{i\uparrow}\rangle \\ &= \frac{U}{2}\sum_n \langle [u_{n\downarrow}(i)\eta_n + v_{n\downarrow}^*(i)\eta_n^\dagger][u_{n\uparrow}(i)\eta_n - v_{n\uparrow}^*(i)\eta_n^\dagger]\rangle \\ &= \frac{U}{2}\sum_n [v_{n\downarrow}^* u_{n\uparrow} f(E_n) - u_{n\downarrow} v_{n\uparrow}^* f(-E_n)]. \end{aligned} \tag{C9}$$

We notice that if $(u_{n\uparrow}, u_{n\downarrow}, v_{n\uparrow}v_{n\downarrow})$ is the solution to the BdG equation with eigenvalue E_n, then $(-v_{n\uparrow}^*, v_{n\downarrow}^*, -u_{n\uparrow}^*, u_{n\downarrow}^*)$ is the solution to the same equation with eigenvalue $-E_n$. Using this symmetry, we can simplify the BdG equation as

$$\sum_j \begin{pmatrix} h_{ij\uparrow} & \delta_{ij} \\ \delta_{ij}^* & -h_{ij\downarrow} \end{pmatrix} \begin{pmatrix} u_{n\uparrow}(j) \\ v_{n\downarrow}(j) \end{pmatrix} = E_n \begin{pmatrix} u_{n\uparrow}(i) \\ v_{n\downarrow}(i) \end{pmatrix}. \tag{C10}$$

Accordingly, we can get self-consistent conditions,

$$\begin{aligned} \langle n_{i\uparrow}\rangle &= \sum_n |u_{n\uparrow}(i)|^2 f(E_n), \\ \langle n_{i\downarrow}\rangle &= \sum_n |v_{n\downarrow}(i)|^2 f(-E_n), \\ \Delta(i) &= U\sum_n v_{n\downarrow}^* u_{n\uparrow} f(E_n), \end{aligned} \tag{C11}$$

In Fig. 10, we use mean-field approximation to study FFLO states. In Fig. 10(a), $\Delta(i)$ fluctuates around $\Delta(i) = 0$, indicating it is a FFLO state. The corresponding local spin polarization m_i is shown in Fig. 10(b), which is similar to the DMRG results in the main text. The Fourier transform of $\Delta(i)$ and m_i in Figs. 10(c) and 10(d) have two peaks at $q/\pi = 0.29$ and $q/\pi = 0.76$, which is also consistent with the results in the main text.

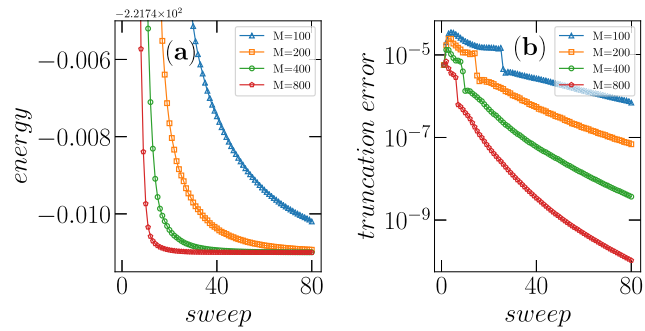

FIG. 11. Ground-state energy for different states and sweeps in (a). Truncation error for different states and sweeps in (b). $L = 120$, $n = 5/12$, $U/t = 1.0$, $V/t = 2.0$, $\alpha = (\sqrt{5}-1)/2$, and $\phi = 0.0$.

APPENDIX D: TRUNCATION ERROR IN THE DMRG CALCULATIONS

In order to illustrate that 800 states (bond dimension) and 80 sweeps are large enough to meet the accuracy requirements in the DMRG calculations, we show the ground-state energy and truncation error for different states and sweeps in Figs. 11(a) and 11(b). Obviously, when sweep = 80 and bond dimension $M = 800$, the ground-state energy converges and the truncation error is less than 10^{-9}.

APPENDIX E: FINITE-SIZE EFFECT

In order to illustrate that the size effect is small for $L = 120$, we show $\overline{S}$ as a function of V/t for different Ls in Fig. 12(a) and the transition points as a function of $1/L$ in Fig. 12(b). When $L = 48$, the size effect is obvious, but the system is large enough for $L = 120$ and the critical points indicated by $\overline{S}$ for $L = 120$ are approximately equal to those for larger sizes $L = 180$ and $L = 240$, indicating that the size effect can be ignored for $L = 120$. Furthermore, we also show η_{FFLO} and $\eta_{\mathrm{CDW}} \cdot \eta_{\mathrm{FFLO}}$ as a function of $1/L$ in Figs. 12(c) and 12(d), which shows that the exponents largely converge when $L > 80$. It is worth noting that this is not contrary to the Imry-Ma-type argument [33], since we adopt a quasiperiodic Zeeman field and the Imry-Ma-type argument is circumvented [34].

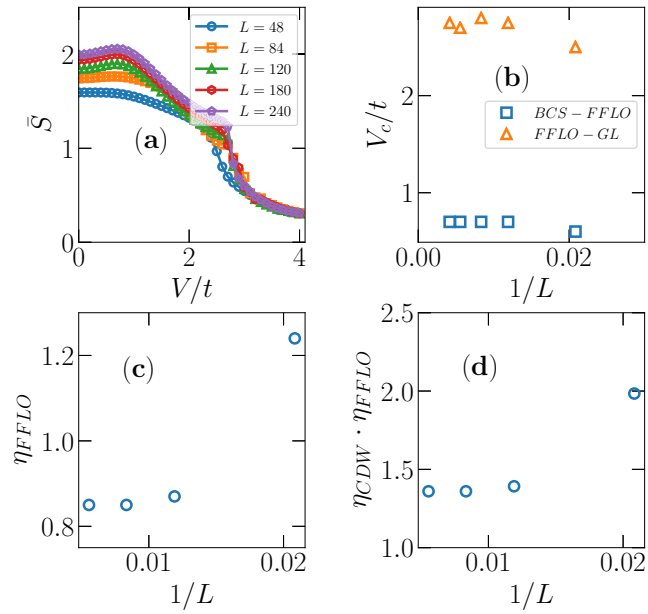

FIG. 12. Entanglement entropy $\overline{S}$ as a function of V/t for different Ls in (a) and the transition points as a function of $1/L$ in (b). The exponent of the pair-pair correlation function η_{FFLO} as a function of $1/L$ in (c). $\eta_{\mathrm{CDW}} \cdot \eta_{\mathrm{FFLO}}$ as a function of $1/L$ in (d). $n = 5/12$, $U/t = 1.0$, $\alpha = (\sqrt{5} - 1)/2$, and $\phi = 0.0$. $V/t = 2$ in (c) and (d).

[1] J. Bardeen, L. N. Cooper, and J. R. Schrieffer, Phys. Rev. **108**, 1175 (1957).
[2] G. Sarma, J. Phys. Chem. Solids **24**, 1029 (1963).
[3] P. Fulde and R. A. Ferrell, Phys. Rev. **135**, A550 (1964).
[4] A. I. Larkin and Y. N. Ovchinnikov, Zh. Eksp. Teor. Fiz. **47**, 1136 (1964).
[5] J. J. Kinnunen, J. E. Baarsma, J.-P. Martikainen, and P. Törmä, Rep. Prog. Phys. **81**, 046401 (2018).
[6] M. Pini, P. Pieri, and G. Calvanese Strinati, Phys. Rev. Research **3**, 043068 (2021).
[7] X.-W. Guan, M. T. Batchelor, and C. Lee, Rev. Mod. Phys. **85**, 1633 (2013).
[8] P. A. Lee, Phys. Rev. X **4**, 031017 (2014).
[9] C. Cho, J. Lyu, C. Y. Ng, J. J. He, K. T. Lo, D. Chareev, T. A. Abdel-Baset, M. Abdel-Hafiez, and R. Lortz, Nat. Commun. **12**, 3676 (2021).
[10] R. Lortz, Y. Wang, A. Demuer, P. H. M. Böttger, B. Bergk, G. Zwicknagl, Y. Nakazawa, and J. Wosnitza, Phys. Rev. Lett. **99**, 187002 (2007).
[11] K. W. Song and A. E. Koshelev, Phys. Rev. X **9**, 021025 (2019).
[12] J. Wosnitza, Ann. Phys. **530**, 1700282 (2018).
[13] A. Bianchi, R. Movshovich, C. Capan, P. G. Pagliuso, and J. L. Sarrao, Phys. Rev. Lett. **91**, 187004 (2003).
[14] Y. Matsuda and H. Shimahara, J. Phys. Soc. Jpn. **76**, 051005 (2007).
[15] P. W. Anderson, J. Phys. Chem. Solids **11**, 26 (1959).
[16] A. Kapitulnik and G. Kotliar, Phys. Rev. Lett. **54**, 473 (1985).
[17] P. W. Anderson, Phys. Rev. **109**, 1492 (1958).
[18] F. Zhou and B. Spivak, Phys. Rev. Lett. **80**, 5647 (1998).
[19] Q. Cui and K. Yang, Phys. Rev. B **78**, 054501 (2008).
[20] Y. L. Loh and N. Trivedi, Phys. Rev. Lett. **104**, 165302 (2010).
[21] A. Lowe, V. Kagalovsky, and I. V. Yurkevich, Phys. Rev. Research **3**, 033059 (2021).
[22] K. Zhao, H. Lin, X. Xiao, W. Huang, W. Yao, M. Yan, Y. Xing, Q. Zhang, Z. Li, S. Hoshino *et al.*, Nat. Phys. **15**, 904 (2019).
[23] M. N. Gastiasoro and B. M. Andersen, Phys. Rev. B **98**, 184510 (2018).
[24] M. Leroux, V. Mishra, J. P. C. Ruff, H. Claus, M. P. Smylie, C. Opagiste, P. Rodière, A. Kayani, G. D. Gu, J. M. Tranquada, W.-K. Kwok, Z. Islam, and U. Welp, Proc. Natl. Acad. Sci. USA **116**, 10691 (2019).
[25] A. P. Petrovic, D. Ansermet, D. Chernyshov, M. Hoesch, D. Salloum, P. Gougeon, M. Potel, L. Boeri, and C. Panagopoulos, Nat. Commun. **7**, 12262 (2016).
[26] B. Sacépé, C. Chapelier, T. I. Baturina, V. M. Vinokur, M. R. Baklanov, and M. Sanquer, Phys. Rev. Lett. **101**, 157006 (2008).
[27] Y. Dubi, Y. Meir, and Y. Avishai, Nature (London) **449**, 876 (2007).
[28] L. Jiang, L. O. Baksmaty, H. Hu, Y. Chen, and H. Pu, Phys. Rev. A **83**, 061604(R) (2011).
[29] J. Li and C. S. Ting, Phys. Rev. B **85**, 094520 (2012).
[30] S. Aubry and G. André, Ann. Isr. Phys. Soc. **3**, 133 (1980).
[31] G. Roux, T. Barthel, I. P. McCulloch, C. Kollath, U. Schollwöck, and T. Giamarchi, Phys. Rev. A **78**, 023628 (2008).
[32] T. Roscilde, Phys. Rev. A **77**, 063605 (2008).
[33] Y. Imry and S.-k. Ma, Phys. Rev. Lett. **35**, 1399 (1975).
[34] H. J. Changlani, N. M. Tubman, and T. L. Hughes, Sci. Rep. **6**, 31897 (2016).

[35] M. Tezuka and A. M. García-García, Phys. Rev. A **82**, 043613 (2010).
[36] I. Zapata, B. Wunsch, N. T. Zinner, and E. Demler, Phys. Rev. Lett. **105**, 095301 (2010).
[37] S. R. White, Phys. Rev. Lett. **69**, 2863 (1992).
[38] B. Bauer, L. D. Carr, H. G. Evertz, A. Feiguin, J. Freire, S. Fuchs, L. Gamper, J. Gukelberger, E. Gull, S. Guertler, A. Hehn, R. Igarashi, S. V. Isakov, D. Koop, P. N. Ma, P. Mates, H. Matsuo, O. Parcollet, G. Pawłowski, J. D. Picon, L. Pollet, E. Santos, V. W. Scarola, U. Schollwöck, C. Silva, B. Surer, S. Todo, S. Trebst, M. Troyer, M. L. Wall, P. Werner, and S. Wessel, J. Stat. Mech.: Theory Exp. (2011) P05001.
[39] M. Dolfi, B. Bauer, S. Keller, A. Kosenkov, T. Ewart, A. Kantian, T. Giamarchi, and M. Troyer, Comput. Phys. Commun. **185**, 3430 (2014).
[40] M. Rizzi, M. Polini, M. A. Cazalilla, M. R. Bakhtiari, M. P. Tosi, and R. Fazio, Phys. Rev. B **77**, 245105 (2008).
[41] A. E. Feiguin and F. Heidrich-Meisner, Phys. Rev. B **76**, 220508(R) (2007).
[42] G. G. Batrouni, M. H. Huntley, V. G. Rousseau, and R. T. Scalettar, Phys. Rev. Lett. **100**, 116405 (2008).
[43] V. V. França, Physica A **475**, 82 (2017).
[44] A. Lüscher, R. M. Noack, and A. M. Läuchli, Phys. Rev. A **78**, 013637 (2008).
[45] F. Heidrich-Meisner, G. Orso, and A. E. Feiguin, Phys. Rev. A **81**, 053602 (2010).
[46] A.-H. Chen and G. Xianlong, Phys. Rev. B **85**, 134203 (2012).
[47] M. Tezuka and M. Ueda, Phys. Rev. Lett. **100**, 110403 (2008).
[48] X. Wei, C. Gao, R. Asgari, P. Wang, and G. Xianlong, Phys. Rev. A **98**, 023631 (2018).
[49] H. Mosadeq and R. Asgari, Phys. Rev. B **91**, 085126 (2015).
[50] T. Giamarchi, *Quantum Physics in One Dimension* (Clarendon Press, Oxford, 2003).
[51] M. Guerrero, G. Ortiz, and J. E. Gubernatis, Phys. Rev. B **62**, 600 (2000).
[52] K. Yang, Phys. Rev. B **63**, 140511(R) (2001).
[53] S. Pilati and S. Giorgini, Phys. Rev. Lett. **100**, 030401 (2008).
[54] D. E. Sheehy and L. Radzihovsky, Ann. Phys. **322**, 1790 (2007).
[55] M. Singh and G. Orso, Phys. Rev. Research **2**, 023148 (2020).
[56] P. Łydżba and T. Sowiński, Phys. Rev. A **101**, 033603 (2020).
[57] R. P. Hardikar and R. T. Clay, Phys. Rev. B **75**, 245103 (2007).
[58] K.-M. Tam, S.-W. Tsai, D. K. Campbell, and A. H. Castro Neto, Phys. Rev. B **75**, 161103(R) (2007).
[59] R. T. Clay and R. P. Hardikar, Phys. Rev. Lett. **95**, 096401 (2005).
[60] M. Tezuka, R. Arita, and H. Aoki, Phys. Rev. Lett. **95**, 226401 (2005).
[61] T. Roscilde, M. Rodríguez, K. Eckert, O. Romero-Isart, M. Lewenstein, E. Polzik, and A. Sanpera, New J. Phys. **11**, 055041 (2009).
[62] A. Moreo and D. J. Scalapino, Phys. Rev. Lett. **98**, 216402 (2007).
[63] T. D. Kühner, S. R. White, and H. Monien, Phys. Rev. B **61**, 12474 (2000).
[64] Y. Liao, A. S. C. Rittner, T. Paprotta, W. Li, G. B. Partridge, R. G. Hulet, S. K. Baur, and E. J. Mueller, Nature (London) **467**, 567 (2010).
[65] R. Nanguneri, M. Jiang, T. Cary, G. G. Batrouni, and R. T. Scalettar, Phys. Rev. B **85**, 134506 (2012).
[66] G. Jotzu, M. Messer, F. Görg, D. Greif, R. Desbuquois, and T. Esslinger, Phys. Rev. Lett. **115**, 073002 (2015).
[67] M. Schreiber, S. S. Hodgman, P. Bordia, H. P. Lüschen, M. H. Fischer, R. Vosk, E. Altman, U. Schneider, and I. Bloch, Science **349**, 842 (2015).
[68] G. Roati, C. D'Errico, L. Fallani, M. Fattori, C. Fort, M. Zaccanti, G. Modugno, M. Modugno, and M. Inguscio, Nature (London) **453**, 895 (2008).
[69] D. E. Sheehy and L. Radzihovsky, Phys. Rev. Lett. **96**, 060401 (2006).